Dispersed clusters in (Fe, Cr)$_3$Al alloys: Neutron time-of-flight diffraction study

Anatoly M. Balagurov,[1,2] Ivan A. Bobrikov,[1] Sergey V. Sumnikov,[1,2] and Igor S. Golovin[3]
[1]*Frank Laboratory of Neutron Physics, Joint Institute for Nuclear Research, 141980 Dubna, Russia*
[2]*Lomonosov Moscow State University, 119991 Moscow, Russia*
[3]*National University of Science and Technology "MISIS," 119049 Moscow, Russia*

(Received 14 August 2018; published 17 January 2019)

The structure and microstructure of Fe-xAl-yCr alloys with $x = 25$ and 27 and $0 \leqslant y \leqslant 15$ have been studied by neutron diffraction at several fixed temperatures with high $\Delta d/d$ resolution and with high-intensity continuous scanning in a wide temperature range. The joint analysis of the obtained data established that the microstructure of these compounds is organized in the form of nanoscopic-sized clusters with an ordered atomic structure coherently embedded in a disordered (or less ordered) matrix. In the quenched samples, the matrix is a disordered A2 phase with clusters of a partially ordered B2 phase, whereas, in the annealed samples, the clusters of the ordered $D0_3$ phase are dispersedly distributed in the B2 matrix. The characteristic size of the clusters depends on the state of the alloy, the chromium content, and the temperature and ranges in size from 100 to 1000 Å. For the matrix, the coherent scattering domain size exceeds 3500 Å. Therefore, the state of the alloys is actually a two-phase state, A2 + B2 or B2 + $D0_3$, although these phases are indistinguishable in elemental composition. One of the factors stabilizing the phase-separated state in a compositionally homogeneous medium can be local composition fluctuations at the level of elementary cells, which in turn lead to fluctuations in the interactions of neighboring pairs of atoms.

DOI: 10.1103/PhysRevMaterials.3.013608

I. INTRODUCTION

It is well known that many physical and engineering properties of alloys highly depend on their particular microstructure, which generally refers to any deviation in the arrangement of atoms from a perfect long-range crystalline order. In addition to the finite crystallite sizes, internal stresses, texture, vacancies, etc., for ordered alloys, the organization of regions with an ordered atomic arrangement is also included in the concept of a microstructure.

Existent experimental data (x-ray diffraction and electron microscopy) allowed the formulation of two basic models, within which structurally ordered regions in alloys are usually considered. Namely, it is assumed that, depending on the conditions for the preparation of the alloy and its subsequent heat treatment, the ordered regions can be either antiphase domains (APDs) or clusters of relatively small (nano- or mesoscopic) dimensions embedded in a structurally disordered matrix. The degree of ordering within domains and clusters can vary from zero to one.

The model of APDs was introduced on the basis of x-ray studies [1] of the ordered Cu_3Au alloy (or Cu-25Au, if the standard for alloy notation is used), in which specific additional broadening of some ("superstructure") peaks with respect to the remaining ("fundamental") peaks has been observed. The effect of APDs on the diffraction pattern was considered in detail in [2], where for Cu_3Au the necessary formulas were obtained and a comparison with experiment was made. In these papers, APDs meant neighboring regions with the same arrangement of atoms that had shifted relative to each other by the part of some lattice translation vector.

The possibility of forming antiphase domains in ordered alloys was subsequently justified theoretically and confirmed by various observations and calculations. It has become generally accepted due to repeated discussion in articles and monographs (e.g., [3,4]). Most of the observations of APDs and coherent boundaries between them are performed using transmission electron microscopy (TEM). A detailed analysis of x-ray-diffraction data (the whole powder pattern modeling (WPPM) method was used) obtained on a specially prepared Cu_3Au alloy was carried out in [5], where various variants of the APDs formation were considered.

The first substantiated indications of the possibility to form an alloy microstructure as small clusters with an ordered atomic structure embedded into a disordered matrix were obtained as a result of computer simulation of short-range order in Cu_3Au [6]. The analysis [7] of diffuse x-ray scattering in CuAu and Cu_3Au also showed good agreement with the cluster model. In Fe-Al-based alloys, dispersed clusters of small (20 to 50 Å) sizes of the ordered $D0_3$ phase in a matrix having the α-Fe structure (disordered A2 phase) were observed (TEM) in compositions with ~20 at. % Al in [8,9], where such a microstructure was designated as a specific K state. Theoretical and experimental efforts of studying the inhomogeneous cluster state were intensified recently, which has been promoted by finding the mixed phase states A2 + $D0_3$, B2 + $D0_3$, and B2 + $D0_{19}$ and the detection of record magnetostriction peaks in the Fe-x Ga alloys at $x \approx 19$ and 27 (see, for instance, [10–13]).

Thus, from the experimental data, it follows that at least in some alloys two alternative versions of the microstructure organization are possible: APDs or ordered clusters in the disordered matrix (OCDM), and their implementation depends on the conditions for the preparation of the alloy. An APD probably is the state closest to equilibrium, whereas an OCDM can be far from equilibrium and

under certain conditions will gradually convert to the APD state.

It is intuitively clear that the cluster state of the crystal microstructure should lead to the broadening of the diffraction peaks. Indeed, in our recent paper [14], neutron-diffraction data have been obtained for the Fe-26.5Al as-cast alloy, from which it follows that the widths of superstructure peaks exceed the widths of fundamental ones by ten or more times. This result was confirmed then by the analysis of neutron diffraction from the Fe-27Al single crystal [15]. In both papers, the combination of high-resolution neutron diffraction and real-time thermodiffractometry was used for experiments. This made it possible to trace the temperature evolution of the structural characteristics of the samples and determine the widths of the great number of fundamental and superstructure diffraction peaks. It was shown that the model of dispersed clusters quite adequately describes the observed diffraction effects and, conversely, some important consequences of the APDs model in these experiments were not observed.

In the present paper, this technique was used to analyze several samples with compositions close to Fe-25Al and doped with chromium. We successfully showed that in the initial (quenched) state the microstructure of these compounds is a matrix of the disordered A2 phase with clusters of the partially ordered B2 phase dispersed in it. After slow heating and cooling, the matrix converted to the B2 phase and the clusters consisted of the almost completely ordered $D0_3$ phase.

It should be noted that the concept of structurally ordered clusters in alloys is not strictly defined. Computer modeling of the ordering process predicts the appearance of interpenetrating volumes with diffuse boundaries and complex topology. In the present paper, the concept of a cluster is used in the diffraction sense; namely, a cluster is understood to be a region, the degree of atomic order of which is higher than in the matrix, which leads to the appearance of superstructure diffraction peaks. The set of such regions can be assigned a certain characteristic size, which determines the additional (size) contribution to the widths of the diffraction peaks.

The physical properties and the phase diagram of the Fe_xAl compositions with $x \approx 3$ (iron aluminide, Fe-25Al), as well as the structure of the ordered phases in this compound, are well studied and widely represented in the literature (see, for instance, [16,17]). For $(Fe, Cr)_3Al$, it is only known that chromium doping somewhat complicates the ordering of the atoms, thereby increasing the plasticity of the alloys, and has a marked effect on the temperature dependences of internal friction [18], which are sensitive to the mobility of dislocations. The material-science characteristics of the $(Fe, Cr)_3Al$ compounds are not discussed here since the results of their studies are detailed in a review [16], a monograph [19], and our recent paper [20].

II. MATERIALS AND EXPERIMENTAL METHOD

In this paper, we present the results obtained for four Fe-xAl-yCr alloys—the nominal and chemical composition, initial state, and room-temperature unit-cell parameter of which are listed in Table I. As-cast samples were obtained by melting the corresponding mixture of pure Fe, Al, and Cr in an induction furnace with an argon atmosphere and subsequently crystallized in a copper cup. The chemical composition of the ingots was examined using energy-dispersive spectroscopy with an accuracy of ±0.2%. For neutron experiments, parallelepipeds with dimensions 4 × 8 × 50 mm were cut from ingots.

TABLE I. Nominal and chemical compositions (in at. %), initial phase states, space groups, and lattice constants of studied samples

Sample	Fe	Al	Cr	Initial state	a, Å
Fe-27Al (S1)	73.5	26.5		$D0_3$, $Fm3m$	5.7969
Fe-27Al-3Cr (S2)	70.3	27.0	2.7	B2, $Pm3m$	2.8956
Fe-25Al-9Cr (S3)	64.6	27.0	8.4	B2, $Pm3m$	2.8954
Fe-25Al-15Cr (S4)	60.3	25.0	14.7	B2, $Pm3m$	2.8972

Neutron-diffraction patterns were measured with a high-resolution Fourier diffractometer (HRFD) operating at the IBR-2 pulsed reactor at JINR (Dubna) [21,22], which is a time-of-flight (TOF) instrument with a fast Fourier chopper. The HRFD can be easily switched between high-resolution ($\Delta d/d \approx 0.0015$) and high-intensity ($\Delta d/d \approx 0.015$) diffraction modes ($d$ is the interplanar distance), which is extremely useful for a joint analysis of the changes in the atomic structure and microstructure of the material in the course of phase transitions (see also [23]).

For Fe-Al alloys similar in composition to Fe-25Al, three structural states are possible and are designated in the phase diagrams as A2, B2, and $D0_3$. In the A2 phase ($Im3m$) there is no ordering, while the Fe and Al atoms with probabilities of 0.75 and 0.25, respectively, occupy two positions in the unit cell. In the B2 phase, Fe atoms can completely fill one of the two possible positions in the $Pm3m$ group, and in the second position Fe and Al are present in equal amounts. In the $D0_3$ phase ($Fm3m$), almost complete ordering is possible. The lattice constants of the states $D0_3$, B2, and A2 are related as $a_{D03} \leqslant 2a_{B2} \leqslant 2a_{A2} \approx 5.80$ Å

The ordering in Fe-Al alloys leads to the appearance of superstructure peaks in neutron-diffraction patterns, the intensity of which is proportional to $(b_{Fe} - b_{Al})^2$, where $b_{Fe} = 0.945$ and $b_{Al} = 0.345$ (in units of 10^{-12} cm) are the coherent neutron-scattering lengths ($b_{Cr} = 0.364$, which is very close to b_{Al}). The relatively large difference between b_{Fe} and b_{Al} provides the sufficiently high intensity of these peaks. In the presence of long-range ferromagnetic order in the alloy, in all diffraction peaks (including superstructure ones) up to temperatures of about 550 °C, there is some magnetic contribution modulated by the magnetic form factor of iron. Owing to the small magnitude of the iron-ordered magnetic moment ($\mu_{Fe} \leqslant 2\mu_B$), this contribution is quite small. Examples of high-resolution diffraction patterns measured in the initial state of Fe-27Al ($D0_3$ phase) and Fe-25Al-15Cr (B2 phase) are shown in Fig. 1. For the disordered A2 phase, the 111, 200, 311, etc., superstructure peaks are absent.

III. DIFFRACTION PEAKS WIDTH FOR THE APDS AND OCDM MODELS

The crystal microstructure manifests itself in the geometrical characteristics of the diffraction peaks: the amplitude (area), width, position, and shape. After their analysis one can

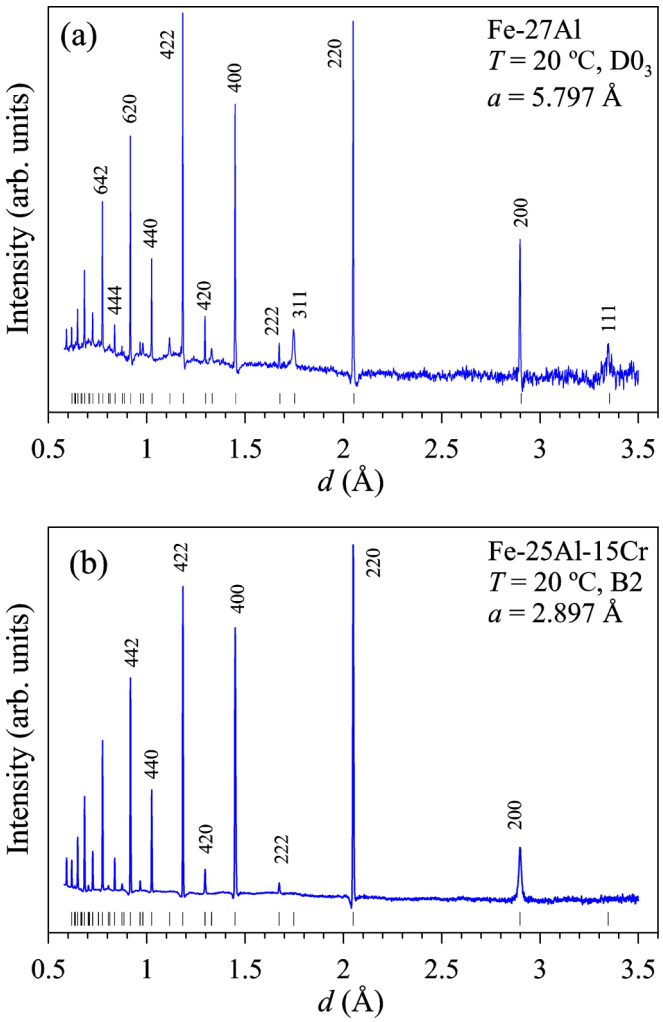

FIG. 1. High-resolution neutron-diffraction patterns of the Fe-27Al and Fe-25Al-15Cr alloys measured in their initial state (before heating). The Fe-27Al sample is in the D0$_3$ phase with 111 and 311 superstructure peaks. The Fe-25Al-15Cr sample is in the B2 phase with 200 and 222 superstructure peaks. Miller indices and vertical bars indicating the positions of the diffraction peaks are in both patterns given for the D0$_3$ unit cell.

make a choice in favor of one or another model. In the case of APDs, the listed characteristics depend also on the type of atomic structure in the alloy and on the particular variant of atomic structure conjugation in neighboring domains.

For the Fe$_3$Al structure, the most probable coherent antiphase domain boundary (APDB) passes along the faces of the cubic unit cell, and the domain shift occurs along the edges of the cube for a half of the D0$_3$ lattice constant. For this phase, the fundamentals are peaks with even Miller indices (h, k, l) satisfying the condition $(h + k + l) = 4n$; they are allowed in all three phases D0$_3$, B2, and A2. The superstructure peaks are divided into two groups: (1) peaks with all even (h, k, l) and with $(h + k + l)/2 = 2n + 1$ (allowed in the phases D0$_3$ and B2) and (2) peaks with all odd (h, k, l) (allowed only in D0$_3$). When the domains are shifted by $a/2$, the size contribution to the broadening of the fundamental and superstructure peaks of the first group and of the superstructure peaks of the second group is different. In the simplest case of diffraction on two neighboring APDs having approximately the same shape and size and separated by a planar coherent APDB, the size contribution to the peak width of these two groups is [15]

$$\Delta d_F \approx d^2/2L_D, \quad \Delta d_S \approx (d^2/L_D)\beta_{hkl}, \tag{1}$$

where $\beta_{hkl} = (h + k + l)/(h^2 + k^2 + l^2)^{1/2}$ (all indices are positive and odd), varying from 1 to 1.73, and, for instance, for the 111 peak $\Delta d_S \approx 3.5\Delta d_F$.

Considering the case of dispersed clusters in compositions of the Fe$_3$Al type, it is clear that two alternative variants are possible and, as shown below, experimentally observed: (1) clusters of the B2 phase in the A2 matrix and (2) clusters of the D0$_3$ phase in the B2 matrix. In this case the peak profiles are determined by the Fourier transform of the shape of the coherently scattering areas in matrix and clusters. Thus, the size contribution to the width of the fundamental and superstructure peaks is

$$\Delta d_F \approx d^2/L_M, \quad \Delta d_S \approx d^2/L_C, \tag{2}$$

where L_M and L_C are the average size of the coherently scattering areas in matrix and clusters. There is the obvious difference between (2) and (1): anisotropic dependence of the width of S peaks on the Miller indices (the β_{hkl} factor) is absent; the ratio between Δd_F and Δd_S can be arbitrary.

For the analysis of the widths of the diffraction peaks, the Williamson-Hall relation is used in this paper, which for a TOF diffractometer can be written in the form [23]

$$(\Delta d)^2 = C_1 + (C_2 + C_3)d^2 + C_4 d^4, \tag{3}$$

where C_1 and C_2 are constants relating to the HRFD resolution function; the microstrain, ε, and average size of coherently scattering areas, $L_{\rm coh}$, are taken into account by $C_3 \approx (2\varepsilon)^2$ and $C_4 \approx (1/L_{\rm coh})^2$, correspondingly. For fundamental or superstructure peaks, either $L_{\rm coh} = L_M$ or L_C must be used. If the size effect is absent, the dependence $(\Delta d)^2$ on d^2 is linear, otherwise it is parabolic. Accordingly, by employing this dependence over a sufficiently large d-spacing range, it is possible to determine both ε and $L_{\rm coh}$.

The restrictions of the Williamson-Hall method are well known (see, for example, [24]). It ignores the distribution of crystallites in size, it makes an arbitrary assumption about how to combine the size and microstrain distributions with the resolution function of the diffractometer, and the determined parameters do not have an exact physical meaning. In particular, Eq. (3) was obtained on the assumption that all distribution functions, including the resolution function of the diffractometer, are Gaussian ones. On the other hand, this method is easy to use and interpret; it makes it possible to detect anisotropy in the peak broadening. Moreover, the determined parameters are not affected by extinction and texture, which, as a rule, are very strong in simple metals. In the particular case of iron-based alloys studied on the TOF diffractometer, the comparatively weak and simple dependence of the HRFD resolution function on d spacing, and the fact that all diffraction peaks are single, also contribute to the success of the analysis.

IV. RESULTS OF DIFFRACTION EXPERIMENTS

From neutron-diffraction patterns, it follows that the initial state of the as-cast sample (Fe-27Al) is the $D0_3$ phase, whereas the quenched samples with Cr are in phase B2 (Fig. 1). For clarity and convenience of comparing the results, the Miller indices for the unit cell of the $D0_3$ phase are used later in the text and in the figures. To acquire the indices of A2 or B2 cells, the indices for $D0_3$ must be divided by 2.

A. Peak widths measured in high-resolution mode

The widths of the peaks (full width at half maximum) were found by describing their profiles in the HRFD high-resolution patterns by an experimentally measured function. This made it possible to determine the microstrains in crystallites at a level of $\varepsilon \approx 4 \times 10^{-4}$ or higher and L_{coh} at a level of 3500 Å or lower.

In Fig. 2, the $(\Delta d)^2$ on d^2 dependences determined for the initial state of the Fe-25Al-9Cr alloy and after its heating to 850 °C and subsequent cooling are shown. It is seen that in the initial state the widths of the peaks with $(h + k + l) = 4n$ (allowed for the A2 phase) fit the linear dependence, whereas, for peaks allowed for the B2 phase, the dependence is parabolic.

After cooling to room temperature, the linear dependence is true for the widths of the peaks with even indices, which are allowed in both A2 and B2 phases (fundamental and superstructure peaks of the first group), while the widths of peaks with odd indices (superstructure peaks of the second group) follow the parabola. Another clearly visible effect is a significant increase (by a factor of ~3) of the L_{coh} after the heating-cooling session.

The Williamson-Hall plots for the Fe-25Al-3Cr and Fe-25Al-15Cr alloys are similar to those shown in Fig. 2. Their comparisons for the fundamental and superstructure peaks are shown in Fig. 3. The widths of the fundamental peaks fit quite well to the general linear dependence, with the exception of certain points measured with Fe-25Al-15Cr, for which the anisotropy of microdeformations is significant.

The size effect for the widths of the fundamental peaks does not appear in any way and, therefore, the L_{coh} for the disordered matrix is larger than the HRFD sensitivity

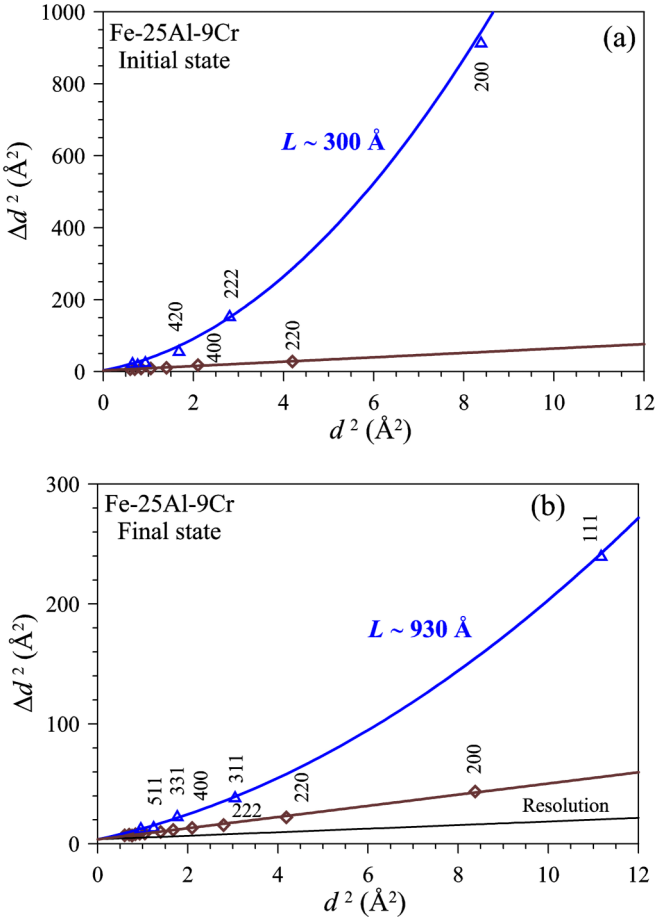

FIG. 2. Comparison of the $(\Delta d)^2$ over d^2 dependences for Fe-25Al-9Cr measured in the initial (before heating) state (B2 phase) and after a heating (to 850 °C) and cooling (to 20 °C) session ($D0_3$ phase). A linear dependence is observed for the matrix peaks, while for superstructure peaks from ordered phases the dependence is parabolic. The statistical errors of experimental points are about the same size as the symbols; the values $(\Delta d)^2$ are multiplied by 10^6. The bottom line shows the diffractometer resolution function.

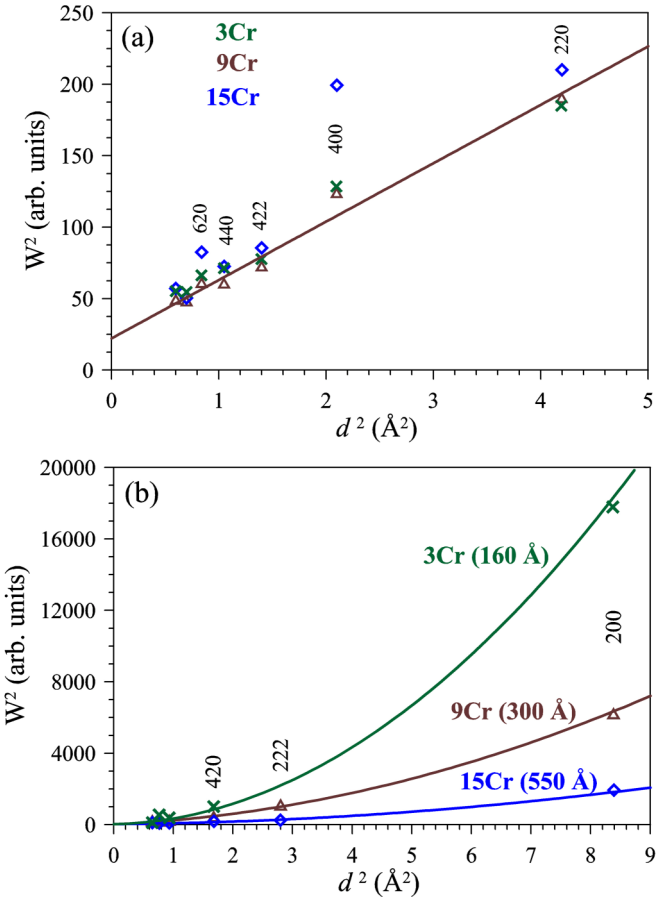

FIG. 3. Williamson-Hall plots for the widths of fundamental (a) and superstructure (b) diffraction peaks measured in the initial state (B2 phase) of samples with Cr content of 3, 9, and 15%. The Miller indices of several first peaks and the characteristic size of clusters are specified. The straight solid line is shown for the sample with 9Cr.

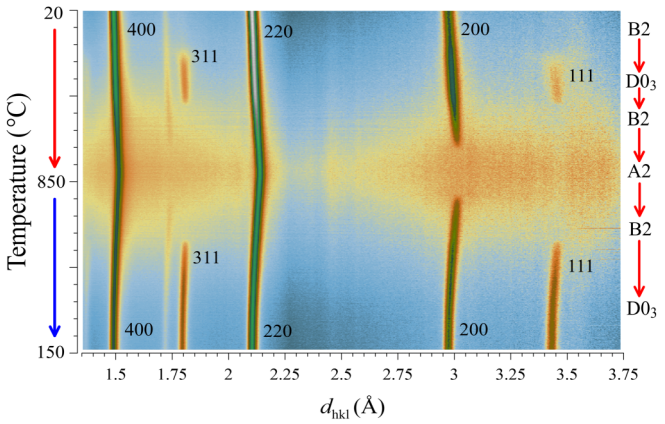

FIG. 4. A 2D visualization of the temperature evolution of diffraction patterns measured upon heating to 850 °C and subsequent cooling for the Fe-25Al-15Cr sample. The phase transitions B2 → $D0_3$ → B2 → A2 at heating and A2 → B2 → $D0_3$ at cooling are seen. The phases are characterized by the 111 and 311 peaks for $D0_3$, by the 200 peak for B2, and by the 220 and 400 peaks for A2. The Miller indices are given for the $D0_3$ unit cell. The heating and cooling rates were slightly different; thus, the number of patterns at equal temperature intervals is somewhat less upon heating.

limit, i.e., $L_M > 3500$ Å. From the parabolic $(\Delta d)^2$ on d^2 dependences for alloys with a chromium content of 3, 9, and 15%, the average cluster sizes were estimated as 160, 300, and 550 Å, respectively. Thus, for compositions with chromium, the ratio of L_M to L_C varies from 6 to 22 (for $L_M = 3500$ Å), which contradicts strongly with the APD model.

B. *In situ* experiments

The samples were heated up to 850 °C at a constant rate of 2.25 K/min. Cooling proceeded linearly with the same rate down to $T \approx 200$ °C; at lower temperatures, the linearity was not maintained. Before heating, at 850 °C, and after cooling to room temperature, high-resolution diffraction patterns were measured. Upon heating of Fe-27Al, a $D0_3$ → B2 → A2 sequence of phase transitions was observed, whereas in all compositions with Cr it was B2 → $D0_3$ → B2 → A2. How these transitions in Fe-25Al-15Cr (and similarly in other compositions with Cr) reveal themselves in the diffraction patterns is shown in Fig. 4, where a short d-spacing range containing peaks from 111 to 400 is presented. In this figure, the characteristic features of structural transitions in these alloys are clearly visible according to the following phenomena: the appearance of an ordered $D0_3$ phase upon heating, the disappearance of all superstructural peaks at higher temperatures with the simultaneous increase of the incoherent background, and the successive appearance of superstructure peaks (first 200, then 111 and 311) upon cooling. The geometrical characteristics of the diffraction peaks determined as functions of temperature at heating and cooling (areas, positions, and widths) were then converted into the following physical quantities: degree of ordering, atomic volume, and characteristics of the microstructure.

Figure 5 illustrates the behavior of the intensities of characteristic diffraction peaks for Fe-25Al-15Cr and Fe-25Al-9Cr

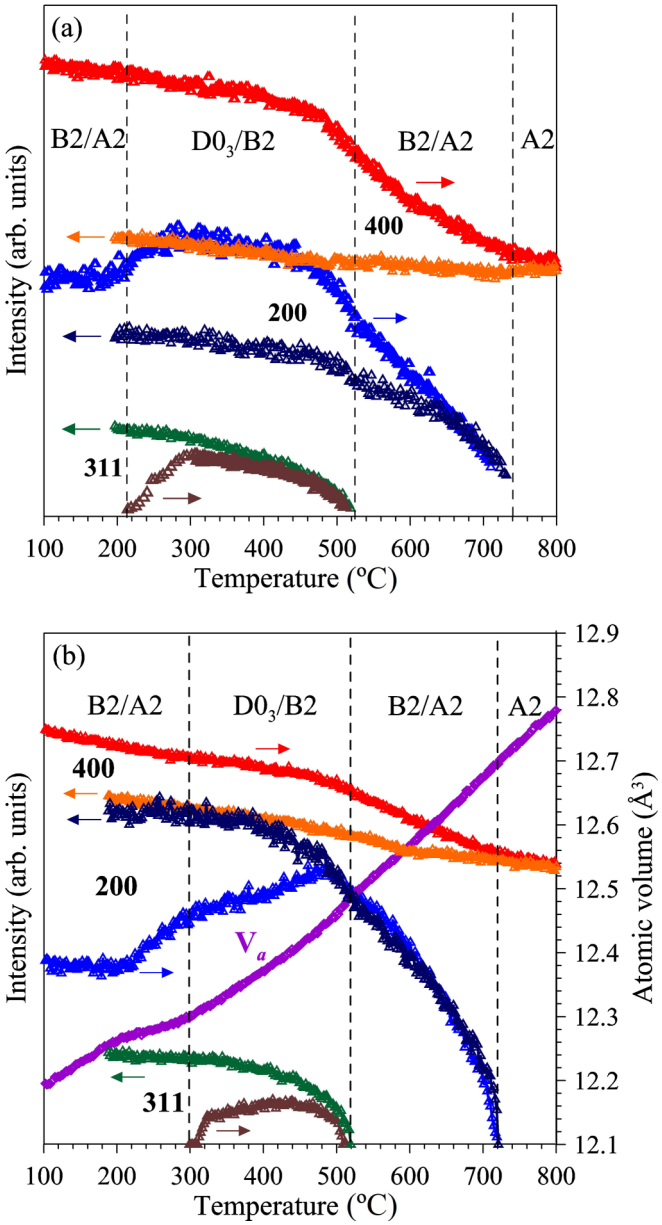

FIG. 5. Intensities of the characteristic diffraction peaks (Miller indices are indicated) in the Fe-25Al-15Cr (a) and Fe-25Al-9Cr (b) samples when heated (arrows to the right) and cooled (arrows to the left). The boundaries between the structural phases (clusters/matrix) as determined from superstructure peaks are indicated by dashed lines. At cooling, both alloys are in the $D0_3$ phase at $T < 200$ °C. For Fe-25Al-9Cr, the behavior of the atomic volume (right scale) upon heating is shown.

compositions upon heating and cooling. The atomic volume of Fe-25Al-9Cr is also shown as a function of temperature. It is seen that the intensities of both the fundamental and superstructure peaks for these compounds (and also for the third composition with Cr) behave in a similar manner. Several features can be noted. The disappearance at heating and appearance at cooling of the superstructure 200 and 311 peaks occur at the same temperatures, i.e., hysteresis is small or absent. Additionally, the 200 peak intensity increases in some temperature range upon heating, the intensity

of the fundamental 400 peak monotonically decreases, and the intensities of all fundamental and superstructure peaks at cooling monotonically increase. The atomic volume during the transitions varies in a continuous manner, which sharply distinguishes these compounds from Fe-27Ga, where the transition from $D0_3$ to A2 goes through the $L1_2$ and $D0_{19}$ phases with different lattice symmetries [23]. However, some changes in the slope of the $V_a(T)$ curve are observed just at temperatures coinciding with the beginning of the increase and decrease of $I(200)$ at $T \approx 200$ and $\approx 520\,^{\circ}\mathrm{C}$, respectively.

The temperature dependences of the widths of the particular diffraction peaks of Fe-25Al-15Cr upon heating are shown in Fig. 6(a). The width of the fundamental peaks (shown for 220) does not change over the entire temperature range, while the widths of superstructure peaks decrease at $T \geqslant 300\,^{\circ}\mathrm{C}$. Above $T \approx 580\,^{\circ}\mathrm{C}$, the width of the 200 peak is close to the contribution from the resolution function. The reduction of the widths of superstructure peaks is naturally associated with an increase in the ordered cluster size. Taking into account the resolution function and using the Scherrer formula ($L \approx d^2/\Delta d$), estimation can be obtained for the average cluster size of the B2 phase in the A2 matrix and its temperature dependence [Fig. 6(b)]. It is seen that the initial size of the clusters depends on the chromium content. The increase in size starts at $T > 350\,^{\circ}\mathrm{C}$ and gradually accelerates until $550\,^{\circ}\mathrm{C}$. At cooling, the dependence of the widths on temperature is practically absent, and their values are close to the values of the resolution function for the corresponding d_{hkl}.

From the ratio of the intensities of the 311 and 220 peaks, the fraction of the sample volume occupied by the $D0_3$ phase can be estimated. Thus, in the S1, S2, S3, and S4 samples at $T = 400\,^{\circ}\mathrm{C}$, the volume fraction occupied by the $D0_3$ phase is about 40, 16, 8, and 4%, respectively, and after heating and cooling it increases by a factor of ~2–2.5. This result corresponds to the fact that an increase in the chromium content reduces the propensity of these alloys to increase their ordering.

One of the changes in the $V_a(T)$ slope (visible in Fig. 5) is shown in more detail in Fig. 7. It illustrates the well-known fact of a decrease of the unit-cell constant under transition between disordered and ordered states (see, for example, [3], p. 215). The analysis of such dependences provides additional useful information on these types of phase transitions, but this is not the subject of this paper.

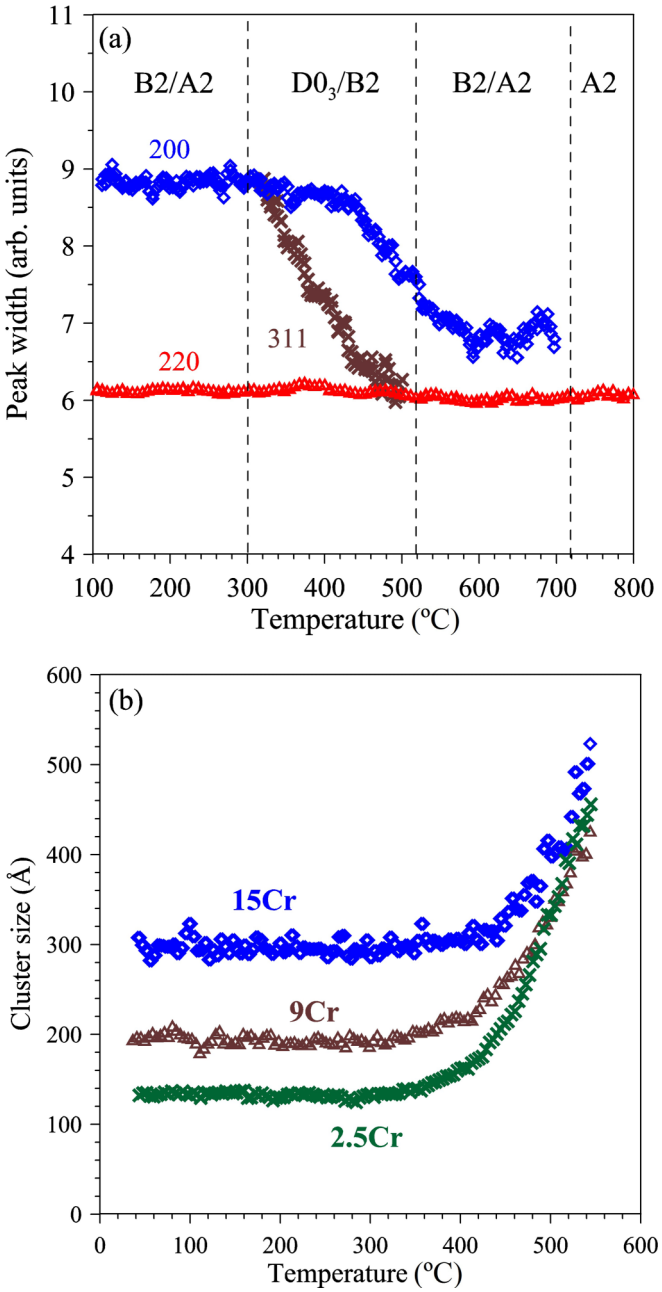

FIG. 6. (a) Widths of the characteristic diffraction peaks of Fe-25Al-15Cr upon heating. (b) Temperature dependences of the average cluster size in the samples with a chromium content of 3, 9, and 15 at. %. Above 550 °C, the cluster size cannot be determined due to the proximity of the width of the peaks to the contribution from the resolution function.

V. DISCUSSION

After the conventional analysis of the diffraction patterns, it could be concluded that in the initial state the Fe-27Al alloy is in the $D0_3$ phase, while all compositions with Cr are in the B2 phase. However, an additional consideration of the diffraction peak widths indicates that the B2 and $D0_3$ ordered phases occupy only a part of the crystallite volume in the form of isolated clusters with a characteristic size of about 100–900 Å imbedded in the A2 or B2 matrix. Thus, the actual state of the samples is a two-phase state: A2 + B2 or B2 + $D0_3$. Upon slow heating of Cr-containing alloys, the following structural transitions occur inside the clusters: B2 → $D0_3$ → B2 → A2; i.e., first, the degree of order increases up to $T \approx 450\,^{\circ}\mathrm{C}$, then it begins to decrease. With subsequent slow cooling, the process goes in the opposite direction: A2 → B2 → $D0_3$.

The observed changes in the intensities of the diffraction peaks belonging to individual phases can be clearly interpreted. For their analysis, it should be taken into account that the intensities of the fundamental (I_F) and superstructure (I_S)

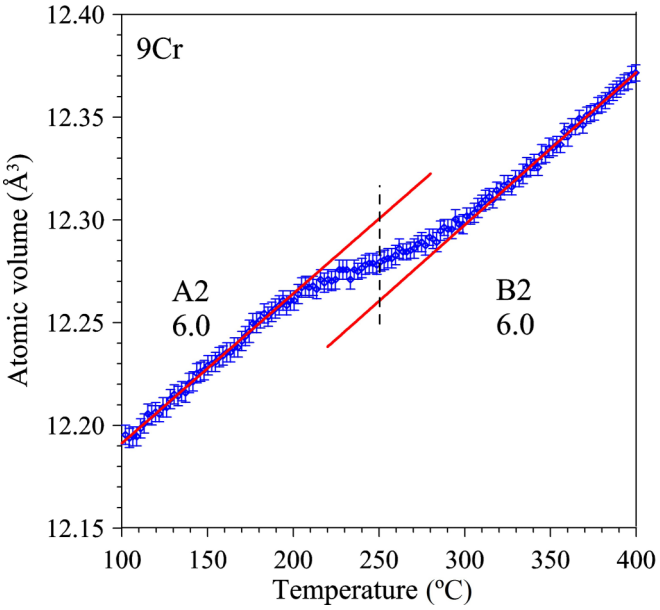

FIG. 7. Temperature dependence of the atomic volume in the region of the A2 → B2 structural transition in the Fe-25Al-9Cr matrix. The straight lines are the result of fitting the experimental points by a linear function in the temperature intervals before and after the transition. The volume expansion coefficients are indicated (in $10^{-5}\,K^{-1}$ units). The volume jump at $T = 250\,^{\circ}C$ is about $0.05\,Å^3$.

peaks depend on temperature such that

$$I_F \sim V_F(T)|F_F|^2 e^{-W(T)}, \quad I_S \sim \xi^2(T)V_S(T)|F_S|^2 e^{-W(T)}, \tag{4}$$

where F_F and F_S are structure factors, $V(T)$ is the volume fraction of a phase, $\xi(T)$ is the degree of atomic ordering, $0 \leqslant \xi(T) \leqslant 1$, and $e^{-W(T)}$ is the Debye-Waller factor. The exponent $W(T)$ includes two terms connected with thermal and static displacements. The first term is the same for matrix and clusters; the second one could be a bit different because of the different degree of ordering in matrix and clusters. For the qualitative analysis of intensities this small difference is not important.

The decrease in the intensity of the 400 peak is related to the Debye-Waller factor and possibly to a partial amorphization of the structure. The comparatively sharp increase in the intensity of the 200 peak at $T \approx 200\,^{\circ}C$ and the appearance of the 311 peak (Fig. 5) do not affect the $I(T)$ dependence of the 400 fundamental peak, which indicates a high degree of coherence of the crystal lattices of the matrix and clusters. Changes in the intensity of the superstructure 200 and 311 peaks are related both to changes in the volume occupied by the matrix and clusters and to the ordering process in them. Upon cooling, the smooth increase in the intensities of the superstructure peaks is also associated with two factors: an increase in the volume occupied by the B2 and $D0_3$ phases and an increase in the degree of atomic ordering in them. Both intensities of superstructure peaks and the atomic volume change continuously upon heating and cooling, indicating that the $D0_3 \leftrightarrow B2 \leftrightarrow A2$ transitions are typical order-disorder transitions of the second order.

The size effect, which manifests itself in the quadratic dependence $(\Delta d)^2$ on d^2, is predicted by both APD and OCDM models, but in the case of APDs these dependencies must be less regular due to the presence of the β_{hkl} factor; additionally, the magnitude of Δd_F and Δd_S should be commensurate. However, the precision of the analysis of the small superstructure peaks is not high enough to identify the influence of β_{hkl}. An additional interfering effect is the microstrain anisotropy. As a result, the deviations of the experimental data points from a regular quadratic dependence are approximately the same for both models. At the same time, a change of Δd_F and Δd_S with increasing Cr content in the very long range is natural for the OCDM model but extremely unlikely in the case of APDs. Moreover, the regular dependence of cluster size on Cr content can be predicted in the frame of the OCDM model.

The absence of obvious temperature dependences of the diffraction peak widths at cooling can be explained by the rapid appearance of clusters with comparatively large sizes ($L \geqslant 1000$ Å) and, correspondingly, by the weak influence of the size factor on the widths measured in the medium resolution mode. A more careful analysis shows a certain increase in the width of the fundamental peaks, i.e., an increase of microstresses, and a slight decrease in the 311 peak width, i.e., an increase in the characteristic size of the $D0_3$ clusters.

The dependence of the atomic volume on temperature (shown in Fig. 7) is calculated from the positions of the fundamental peaks, i.e., they characterize the matrix. This means that the unit-cell parameter of the matrix is sensitive to the ordering processes occurring inside the clusters. Indeed the unit-cell parameters determined from the fundamental and superstructure diffraction peaks coincide with an accuracy of ~0.0005 Å [14]. This value is much smaller than the change in the lattice parameter during the A2 → B2 transition. That is, the ordering preserves a high degree of coherence between the crystal lattices of the matrix and clusters.

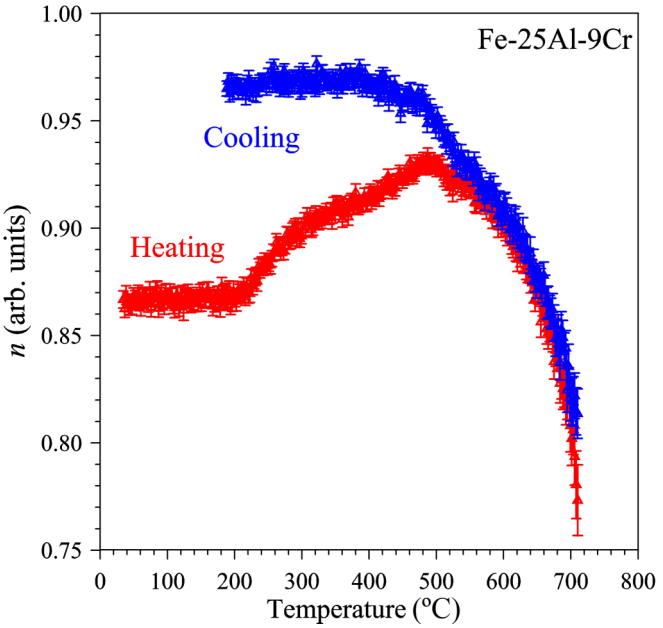

FIG. 8. Temperature dependences of the degree of atomic order inside the clusters in Fe-25Al-9Cr upon heating and cooling.

The ratio of intensities of the reflection orders does not depend on texture effects, which makes it possible to estimate the temperature dependence of cluster ordering degree by using the formulas (4). As an example, it is calculated by analyzing the intensities of the 200 and 400 peaks. Since we do not know the volume occupied by the clusters, the relative behavior of the degree of order can be only obtained from the ratio of intensities. In Fig. 8 this factor is shown for both heating and cooling processes for Fe-25Al-9Cr composition. It is seen that upon slow heating the ordering grows up in the range from 220 to 500 °C. At cooling, the degree of order is markedly higher than in the initial state. For other samples the behavior is similar.

VI. CONCLUSIONS

The presented results clearly indicate that the microstructure of both quenched and annealed alloys of the Fe-Al-Cr system is organized in the form of a matrix with a disordered (or partially ordered) atomic structure and clusters of nanoscopic size with an ordered atomic structure dispersedly embedded in the matrix. The presence of volumes with ordered (B2 or $D0_3$) structures is unambiguously confirmed by neutron-diffraction patterns containing the corresponding superstructure peaks. The characteristic sizes of these volumes depend strongly on the state of the alloy, the chromium content, heat treatment, and the measurement temperature, and range from 160 to 1000 Å. These facts contradict the prediction of uniform ordering of the alloy with the formation of antiphase domains and, conversely, completely correspond to the model of dispersed clusters with an ordered structure. The degree of atomic ordering in the clusters depends on temperature, and after heating and cooling it is markedly higher than in the initial state.

The principal difference between the models of antiphase domains and dispersed clusters can be formulated as follows. The first of them corresponds to a compositionally and crystallographically homogeneous single-phase state that has a specific organization of the microstructure. According to the second model, the studied samples are actually in a two-phase state, B2 + A2 or $D0_3$ + B2, although the elemental composition of these phases is the same. In some papers (see, for example, [25,26]) the coexistence of ordered and disordered phases is denoted as the phase-separated state. This type of inhomogeneity (phase separation) is well known in the physics of complex oxides in which unusual properties are observed. In $La_2CuO_{4+\delta}$ there exists a "chemical" separation resulting in superconducting and antiferromagnetic regions with different contents of extra oxygen [27]. In oxides with the colossal magnetoresistance effect, for instance in $(La_{1-y}Pr_y)_{1-x}Ca_xMnO_3$, "structural and magnetic" phase separation onto mesoscopic regions with different structural and magnetic organization is known to occur [28]. The phase separation in the case of Fe-Al and Fe-Ga systems may be indicated as "order-disorder" in terms of coexisting regions that differ in the degree of atomic order only.

One of the stabilizing factors for a two-phase state in a compositionally homogeneous medium can be local composition fluctuations at the level of unit cells, which in turn leads to fluctuations in interactions in neighboring pairs of atoms. An example of this type of fluctuation in intermetallic compounds is a modified $D0_3$ structure (M-$D0_3$) with increased Ga-Ga pair local concentration, which was suggested and experimentally supported in [29]. The existence of tetragonally modified $D0_3$ nanoinclusions was confirmed recently [30] through a combination of experimental studies, model calculations, and simulations for Fe-17Ga and Fe-17Ga-0.2La compounds. The importance of inhomogeneities for the explanation of the giant magnetostriction in Fe-Ga alloys is becoming increasingly known now. Although direct proofs of the existence of a phase-separated state in the form of a matrix and dispersed clusters are obtained only for the Fe-Al type alloys, there are grounds to believe that similar states are possible in the Fe-Ga compositions. Consequently, the "order-disorder" phase-separated states must be included in any theoretical consideration of this phenomenon.

The obtained results allow us to formulate one more important conclusion. It is the model of dispersed clusters which adequately interprets the experimental results for nonequilibrium states after different heat treatments. In particular, it can lead to reexamination of two-phase ranges of Fe-Me phase diagrams if one of the coexisting phases is an ordered phase.

ACKNOWLEDGMENTS

This work was carried out with support from the Ministry of Education and Science of the Russian Federation in the framework of the Increase Competitiveness Program of the National University of Science and Technology (NUST) "MISiS," implemented by a governmental decree dated 16 March 2013, No. 211. In addition, this work was supported by the Russian Foundation for Basic Research (Projects No. 18-02-00325, No. 18-58-52007, and No. 17-52-44024) and partly by the Russian Scientific Foundation (Project No. 18-12-00283).

[1] F. W. Jones and C. Sykes, Proc. Roy. Soc. A **166**, 376 (1938).
[2] A. J. C. Wilson, Proc. Roy. Soc. A **181**, 360 (1943).
[3] B. E. Warren, *X-Ray Diffraction* (Addison Wesley, New York, 1969).
[4] P. Scardi, in *Powder Diffraction. Theory and Practice*, edited by R. F. Dinnebier and S. J. L. Billinge (The Royal Society of Chemistry, 2008), p. 376.
[5] P. Scardi and M. Leoni, Acta Materialia **53**, 5229 (2005).
[6] P. C. Gehlen and J. B. Cohen, Phys. Rev. **139**, A844 (1965).
[7] M. Greenholz and A. Kidron, Acta Cryst. A **26**, 306 (1970).
[8] H. Warlimont and G. Thomas, Metal. Sci. J. **4**, 47 (1970).
[9] D. Watanabe, H. Morita, H. Saito, and S. Ogawa, J. Phys. Soc. Jpn. **29**, 722 (1970).
[10] O. Ikeda, R. Kainuma, I. Ohnuma, K. Fukamichi, and K. Ishida, J. Alloys and Comp. **347**, 198 (2002).
[11] S. Bhattacharyya, J. R. Jinschek, A. Khachaturyan, H. Cao, J. F. Li, and D. Viehland, Phys. Rev. B **77**, 104107 (2008).
[12] A. G. Khachaturyan and D. Viehland, Metall. Mater. Trans. A **38**, 2308 (2007).

[13] S. Bhattacharyya, J. R. Jinschek, J. F. Li, and D. Viehland, J. Alloys and Comp. **501**, 148 (2010).
[14] A. M. Balagurov, I. A. Bobrikov, B. Mukhametuly, S. V. Sumnikov, and I. S. Golovin, JETP Lett. **104**, 539 (2016).
[15] A. M. Balagurov, I. A. Bobrikov, S. V. Sumnikov, and I. S. Golovin, Acta Mater. **153**, 45 (2018).
[16] N. S. Stoloff, Mater. Sci. Eng. A **258**, 1 (1998).
[17] O. Kubaschewski, in *Iron: Binary Phase Diagrams* (Springer-Verlag, 1982), p. 5.
[18] Z. Belamri, D. Hamana, I. S. Golovin, and I. B. Chudakov, Metallofiz. Noveishie Tekhnol. **35**, 209 (2013).
[19] I. S. Golovin and A. M. Balagurov, *Structure Induced Anelasticity in Iron Intermetallic Compounds and Alloys* (Materials Research Foundations, 2018), Chap. 5, p. 209.
[20] I. S. Golovin, A. Emdadi, A. M. Balagurov, I. A. Bobrikov, J. Cifre, M. Yu. Zadorozhnyy, and A. Rivière, J. Alloys Comp. **746**, 660 (2018).
[21] A. M. Balagurov, Neutron News **16**, 8 (2005).
[22] A. M. Balagurov, I. A. Bobrikov, G. D. Bokuchava, V. V. Zhuravlev, and V. G. Simkin, Phys. Part. Nucl. **46**, 249 (2015).
[23] A. M. Balagurov, I. S. Golovin, I. A. Bobrikov, V. V. Palacheva, S. V. Sumnikov, and V. B. Zlokazov, J. Appl. Cryst. **50**, 198 (2017).
[24] E. J. Mittemeijer and U. Welzel, Z. Kristallogr. **223**, 552 (2008).
[25] S. Allen, Philos. Mag. **36**, 181 (1977).
[26] K. Oki, S. Matsumura, and T. Eguchi, Phase Trans. **10**, 257 (1987).
[27] J. D. Jorgensen, B. Dabrowski, S. Pei, D. G. Hinks, L. Soderholm, B. Morosin, J. E. Schirber, E. L. Venturini, and D. S. Ginley, Phys. Rev. B **38**, 11337 (1988).
[28] E. Dagotto, J. Burgy, and A. Moreo, Solid State Comm. **126**, 9 (2003).
[29] T. A. Lograsso, A. R. Ross, D. L. Schlagel, A. E. Clark, and M. Wun-Fogle, J. Alloys and Comp. **350**, 95 (2003).
[30] Y. He, X. Ke, C. Jiang, N. Miao, H. Wang, J. M. D. Coey, Y. Wang, and H. Xu, Adv. Funct. Mat. **28**, 1800858 (2018).